EurJIC
European Journal of Inorganic Chemistry

Research Article
doi.org/10.1002/ejic.202200439

Chemistry Europe
European Chemical
Societies Publishing

www.eurjic.org

Unique Dimerization Topology and Countercation Binding Modes in 12-Metallacrown-4 Compounds

Elvin V. Salerno,[a] Collin M. Foley,[b] Vittoria Marzaroli,[c] Bernadette L. Schneider,[a] Max D. Sharin,[a] Jeff W. Kampf,[a] Luciano Marchiò,[c] Matthias Zeller,[d] Régis Guillot,[e] Talal Mallah,*[e] Matteo Tegoni,*[c] Vincent L. Pecoraro,*[a] and Curtis M. Zaleski*[b]

Seven dimeric metallacrowns (MC) based on Ln[12-MC$_{M(III)N(shi)}$-4], where Ln^{III} = Dy, Ho, Yb, or Y, M^{III} = Mn or Ga, and shi^{3-} is salicylhydroximate, have been synthesized and characterized by single-crystal X-ray diffraction, and for the dysprosium-manganese dimers, the magnetic properties have been measured. In each dimer two Ln[12-MC$_{M(III)N(shi)}$-4] units are linked by four bridging dicarboxylate anions (isophthalate, trimesate, dinicotinate, or 2,2′-dithiodibenzoate). Three different countercations (sodium, gallium(III), or pyridinium) were used to maintain charge balance of the dimer. While pyridinium does not bind to the dimer, the choice of the dicarboxylate dictates where the countercations Na$^+$ or Ga^{III} bind. With isophthalate and trimesate, the sodium ion binds to the central MC cavity opposite of the Ln^{III}, and with dinicotinate the sodium or gallium(III) ions bind to the pyridyl nitrogen of the dinicotinate. All three Dy$_2$Mn$_8$ dimers exhibit an out-of-phase magnetic susceptibility signal consistent with a shallow barrier to magnetization relaxation.

Introduction

One goal of the synthetic chemist is to gain control over a system so that subtle variations in molecular design allow an investigation on how these changes affect physical and chemical properties from a fundamental perspective. Be the system metal-organic frameworks,[1] quantum dots,[2] perovskite compounds,[3] or coordination complexes,[4] the ability to alter the molecular structure to fine tune properties is the objective of the chemist. Usually, for metal ion containing extended systems (oxides, fluorides, cyanides etc. and coordination networks) and for monometallic complexes, it is possible to modify the nature of the metal ion and maintain the overall structure; thus, inducing changes in the physical properties of the

materials. In multimetallic molecular complexes, modifying the nature of the metal ion has, in most cases, a large impact on the structure preventing a systematic study and rationalization of their physical properties, in particular magnetic, related to the nature of the metal ion. This is also the case for lanthanide multimetallic complexes where luminescence and magnetic properties are targeted. One particular coordination system we have been interested in exploring is metallacrowns (MC), which are multimetallic systems with either only transition metal ions or with mixed transition metal and lanthanide ions systems.[5] These molecules are well suited to minute architectural manipulations as they can self-assemble in solution through templating of anionic ligands, cationic ring transition metal ions, and typically a central lanthanide or transition metal ion.[6] Through careful choice of the metal ion and ligand types and the control of the stoichiometric ratios between components, these molecules can be systemically altered so that the basic structure of the molecule is retained while the physical and chemical properties can be tuned to a particular application. One hallmark of metallacrown chemistry is this ability to make wholesale changes to the synthetic scheme with the ability to predictably maintain the underlying MC bonding motif. Metallacrowns have found varied applications including host-guest binding,[7] magnetorefrigeration,[8] molecular magnetism,[9–16] white-light emission,[17] and luminescence.[18–23]

One area that we have focused on is the relationship of structural manipulations and the fine-tuning of the single-molecule magnetism properties of metallacrowns, which have a relatively large number of paramagnetic metal ions confined to a small molecular volume.[5,6] Single-molecule magnets (SMMs) are systems which exhibit magnetic blocking at a molecular level.[24] Such systems are desirable because they represent, among other things, a potential means for very high-density data storage or quantum bits.[25] Among the chief virtues of molecular magnets is the fact that they are discrete chemical

[a] Dr. E. V. Salerno, B. L. Schneider, M. D. Sharin, Dr. J. W. Kampf, Dr. V. L. Pecoraro
Department of Chemistry,
University of Michigan,
Ann Arbor, Michigan, 48109, United States
E-mail: vlpec@umich.edu

[b] C. M. Foley, Dr. C. M. Zaleski
Department of Chemistry and Biochemistry,
Shippensburg University,
Shippensburg, Pennsylvania 17257, United States
E-mail: cmzaleski@ship.edu

[c] Dr. V. Marzaroli, Dr. L. Marchiò, Dr. M. Tegoni
Department of Chemistry, Life Sciences, and Environmental Sustainability,
University of Parma,
Parco Area delle Scienze 11 A, 43124 Parma, Italy
E-mail: matteo.tegoni@unipr.it

[d] Dr. M. Zeller
Department of Chemistry, Purdue University,
West Lafayette, Indiana 47907, United States

[e] Dr. R. Guillot, Dr. T. Mallah
Institut de Chimie Moléculaire et des Matériaux d'Orsay,
Université Paris Saclay, ICMMO CNRS 8182,
91405 Orsay, Cedex, France
E-mail: talal.mallah@universite-paris-saclay.fr

EurJIC
European Journal of Inorganic Chemistry

Research Article
doi.org/10.1002/ejic.202200439

Chemistry Europe
European Chemical
Societies Publishing

systems, and thus their chemical and magnetic architectures can be manipulated simultaneously to produce desired properties. For synthetic chemists to understand how to design a system of interest rationally, they must grasp the subtle manners in which chemical changes alter magnetic behavior. Therefore, strategic and systematic studies to determine the magnetic effects imposed by subtle chemical alterations are warranted.
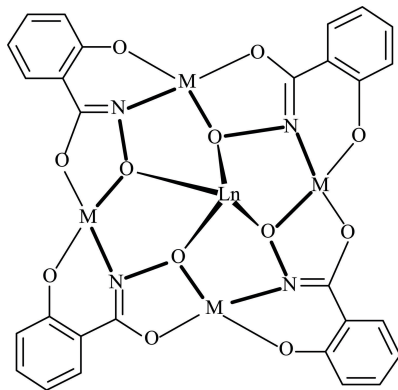
Previously we investigated how the identity of the bridging carboxylate ligand in a series of monomeric 12-MC-4 complexes (Scheme 1) affected the single-molecule magnet properties of these compounds.[9] Utilizing the MC framework ligand salicyl-hydroxamic acid (H_3shi), a series of Dy^{III}-Mn^{III} metallacrowns, Dy[12-$MC_{Mn(III)N(shi)}$-4], were synthesized with the ancillary carboxylate anions acetate, benzoate, trimethylacetate, or salicylate. The four carboxylate anions serve to tether the Dy^{III} to the central MC cavity and bridge the central Dy^{III} to the four ring Mn^{III} ions. It was determined that only the salicylate-linked complexes displayed slow relaxation of the magnetization, one of the hallmarks of single-molecule magnets. This was true even as the countercation, necessary for charge balance, was exchanged for either Na^+ or K^+. The bridging ligand properties were analyzed in the context of the pK_a of the parent carboxylic acid. The pK_a value can serve as a proxy measure of the electronegativity of the bonding conjugate base and, therefore, its electronic donating/withdrawing properties. Notably, the conjugate acid of salicylate had the lowest pK_a of the series at 2.93 while that of benzoate, acetate, and trimethylacetate are 4.20, 4.77, and 5.01, respectively. That study concluded that the electronic donating capacity of the ligand may influence Mn^{III}/Dy^{III} magnetic coupling and hence single-molecule magnet behavior.

Building upon our initial report[26] of LnM(acetate)$_4$ [12-$MC_{Mn(III)N(shi)}$-4], where Ln^{III}=Pr–Yb (except Pm) and Y and M^+=Na or K, Song, Dou, and coworkers also made alterations to the metallacrown assembly.[27] With a diamagnetic central cation, the complex Y(acetate)$_4$[12-$MC_{Mn(III)N(shi)}$-4] did not display SMM behavior, likely due the antiferromagnetic coupling of the ring ions. However, if a $[W^V(CN)_8]^{3-}$ anion was bound to the Y(acetate)$_4$[12-$MC_{Mn(III)N(shi)}$-4] complex the molecule did display SMM behavior. The four cyanide ligands of the octacyanotung-
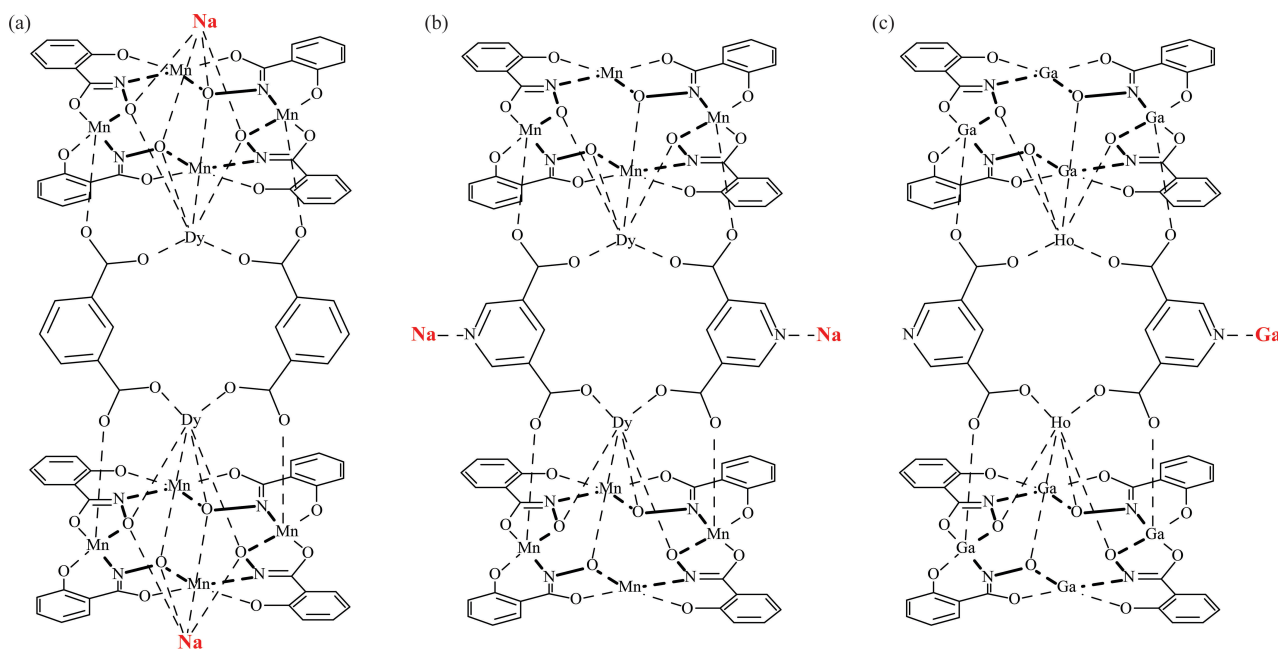
state anion bind to the ring Mn^{III} ions to place the $[W^V(CN)_8]^{3-}$ unit on the concave side of the MC cavity and opposite of the Y^{III} ion. The presence of the paramagnetic $[W^V(CN)_8]^{3-}$ species bridging the Mn^{III} belonging to [12-$MC_{Mn(III)N(shi)}$-4] changed the exchange coupling between the Mn^{III} ions from antiferromagnetic to ferromagnetic leading to high spin ground state presenting a slow relaxation of the magnetization in zero applied DC magnetic field. This example further demonstrates that changes to the MC molecule allow for the fine-tuning and rationalization of the magnetic properties.

We then demonstrated that it was possible to switch the ring Mn^{III} ions with Ga^{III} to produce similar monomeric Ln-(benzoate)$_4$[12-$MC_{Ga(III)N(shi)}$-4] structures,[19] and if the carboxylate anion of the monomeric Ln[12-$MC_{Ga(III)N(shi)}$-4] unit is replaced by a dicarboxylate such as isophthalate (iph^{2-}), two Ln[12-$MC_{Ga(III)N(shi)}$-4] units may be joined together to form a dimer of MCs, {Ln[12-$MC_{Ga(III)N(shi)}$-4]}$_2$(iph)$_4$.[21] The Ln^{III}-Ga^{III} monomers and dimers are highly luminescent in both the visible and near-infrared regions with potential applications such as molecular nanothermometers.[21b] Subsequently we showed that the Ga^{III} of the dimer MC could be replaced with Al^{III}[28] or Mn^{III}[29] ions and the isophthalate could be replaced with iodine[22] or maleimido[30] substituted versions of the dicarboxylate. Liu, Tong *et al.* then expanded upon the reports of the Ln–Mn monomers and the Ln–Ga dimers to examine Dy^{III}-Mn^{III} dimeric and trimeric metallacrowns and investigated the influence of spatial separation of monomeric DyNa[12-$MC_{Mn(III)N(shi)}$-4] complexes on the magnetic behavior.[31] This was accomplished by producing MC dimers and trimers (triangular arrangement) linked by bridges of various lengths, yielding Dy^{III}-Dy^{III} distances of 7.169 Å (isophthalate) and 12.521 Å (4,4'-oxybis[benzoate]) in the two dimers and 10.040 Å (terephthalate) and 14.165 Å ([1,1'-biphenyl]-4,4'-dicarboxylate) in the two triangular trimers. None of these four complexes exhibited slow relaxation of magnetization in the absence of an applied static magnetic field. This includes the isophthalate derivative which is isostructural (however with a different crystal structure) to our compound **1**, which contrarily did show slow relaxation of magnetization (details in Discussion). [The dimer with 4,4'-oxybis[benzoate] displayed a slight frequency-dependent out-of-phase magnetic susceptibility in the presence of a 1000 Oe applied magnetic field.]

The above discussion demonstrates that the MC framework can be altered to accommodate a variety of ring metal ion and ancillary ligand types. This can lead to single-molecule magnet properties for the Ln–Mn systems or luminescent applications for the Ln–Ga systems. Herein we further broaden the scope of the substitution ability of the dimer {Ln[12-$MC_{M(III)N(shi)}$-4]}$_2$ metallacrowns and showcase how we can alter the components of the MC system that affects where countercations can bind to the MC (Scheme 2) and how for a few of the compounds the magnetic properties may be affected by subtle changes to the structure. Using the MC unit of Ln[12-$MC_{M(III)N(shi)}$-4]), where Ln^{III}=Dy, Ho, Yb, or Y and M^{III}=Mn or Ga, we have synthesized a series of dimeric metallacrowns where the bridging dicarboxylate anion linking the two monomers has been altered to determine where the countercation (Na^+ or Ga^{III}) binds to the


Scheme 1. [12-$MC_{Mn(III)N(shi)}$-4] structural unit.

Eur. J. Inorg. Chem. **2022**, e202200439 (2 of 14)

© 2022 Wiley-VCH GmbH

EurJIC
European Journal of Inorganic Chemistry

Research Article
doi.org/10.1002/ejic.202200439

**Chemistry Europe**
European Chemical
Societies Publishing

Scheme 2. Different possible binding sites for Na$^+$ or Ga^{III} countercations to the MC dimer. (a) central MC cavity and (b & c) pyridyl nitrogen atom of dinicotinate. For clarity only 2 of the 4 dicarboxylate anions are shown.

dimer and how this affects the magnetic properties of the Dy^{III}-Mn^{III} dimers. The employed dicarboxylate anions (Scheme 3) include isophthalate (iph^{2-}), trimesate (tma^{2-}), dinicotinate (dnic^{2-}, i.e. pyridine-3,5-dicarboxylate), and 2,2′-dithiodibenzoate (dtba^{2-}). With various combinations of the central lanthanide ion, the ring metal ion, and the bridging dicarboxylate anion, we report the structure and properties of the

dimers {DyNa[12-MC$_{Mn(III)N(shi)}$–4]}$_2$(iph)$_4$(H$_2$O)$_2$(DMF)$_6$·6H$_2$O·4DMF, **Dy$_2$Mn$_8$Na$_2$(iph)$_4$ (1)**; {DyNa[12-MC$_{Mn(III)N(shi)}$–4]}$_2$(tma)$_4$(H$_2$O)$_8$·5H$_2$O·14DMF, **Dy$_2$Mn$_8$Na$_2$(tma)$_4$ (2)**; {DyNa[12-MC$_{Mn(III)N(shi)}$–4]}$_2$(dnic)$_4$(H$_2$O)$_{10}$·4DMF, **Dy$_2$Mn$_8$Na$_2$(dnic)$_4$ (3)**; {YbNa[12-MC$_{Ga(III)N(shi)}$–4]}$_2$(tma)$_4$(H$_2$O)$_{10}$·3H$_2$O·15DMF, **Yb$_2$Ga$_8$Na$_2$(tma)$_4$ (4)**; [Hpy]$_2${Dy[12-MC$_{Ga(III)N(shi)}$–4]}$_2$(dtba)$_4$(py)$_4$·2py·6MeOH, **Dy$_2$Ga$_8$(Hpy)$_2$(dtba)$_4$ (5)**; [Hpy]$_2${Y[12-MC$_{Ga(III)N(shi)}$–4]}$_2$(dnic)$_4$(py)$_6$·
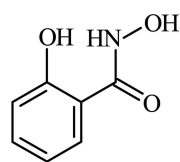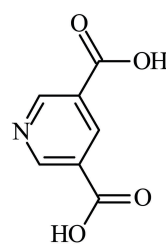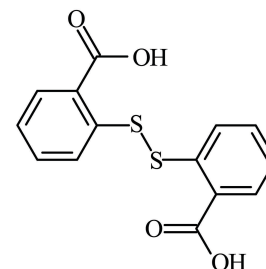

Salicylhydroxamic acid
H$_3$shi
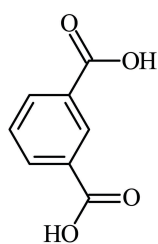
Isophthalic acid
H$_2$iph
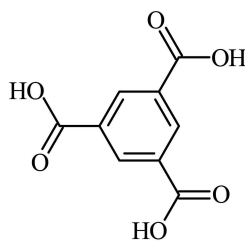
Trimesic acid
H$_2$tma

Dinicotinic acid
H$_2$dnic

2,2′-Dithiobenzoic acid
H$_2$dtba

Scheme 3. Ligands used to generate the investigated dimeric metallacrowns.

EurJIC
European Journal of Inorganic Chemistry

Research Article
doi.org/10.1002/ejic.202200439

Chemistry Europe
European Chemical Societies Publishing

4DMF, **Y$_2$Ga$_8$(Hpy)$_2$(dnic)$_4$** (**6**); and {Ho[12-MC$_{Ga(III)N(shi)}$-4]]}$_2$[Ga-(OH)(DMF)$_4$](dnic)$_4$(H$_2$O)(DMF)$_3$(py)·6DMF, **Ho$_2$Ga$_8$(Ga-OH)(dnic)$_4$** (**7**). We have previously reported the X-ray structure of **1**,[29] but we include the compound here so as to compare its structural features to the other compounds and to report its magnetic behavior, which has not been previously published.
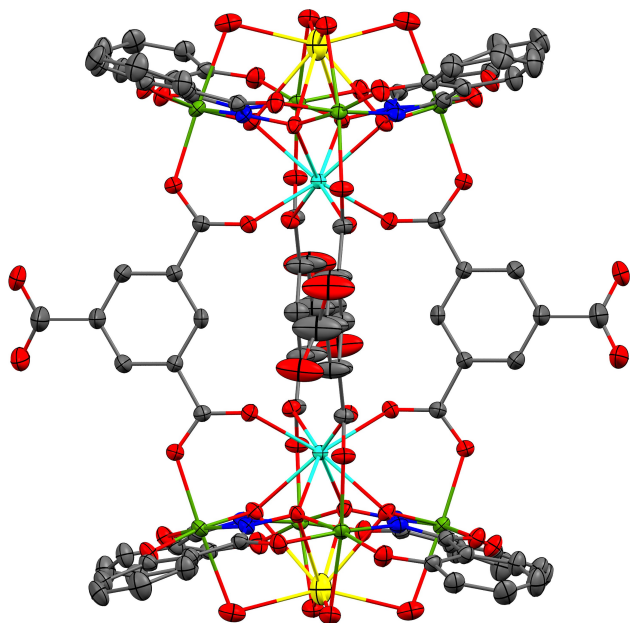
Results and Discussion

Description of Structures

All of the reported structures share a basic structural motif: two Ln[12-MC$_{M(III)N(shi)}$-4] units, where Ln^{III} = Dy, Ho, Yb, or Y and M^{III} = Mn or Ga, are linked via four dicarboxylate anions to form a dimer of the MCs subunits (Figure 1, Figure 2, Figure 3, and Figure 4 and S1–S3; Table S1). Each MC of the dimer is comprised of four shi^{3-} ligands and four M^{III} centers and are charge neutral. The four doubly negative dicarboxylate anions (negative eight overall charge) that bridge the two MCs are partially counterbalanced by two Ln^{III} cations that are captured in the central cavity of each MC. The remaining negative two charge is balanced in by either two Na$^+$ ions (**1–4**), two pyridinium ions (Hpy$^+$; **5&6**), or in one case a Ga^{III}, which is in turn counterbalanced by a hydroxideanion which binds to the same Ga^{III} (**7**). From a synthetic perspective, it is important that charge considerations must be considered when developing

Figure 1. Single-crystal X-ray structure of {DyNa[12-MC$_{Mn(III)N(shi)}$-4]]}$_2$(tma)$_4$(H$_2$O)$_8$·5H$_2$O·14DMF, **Dy$_2$Mn$_8$Na$_2$(tma)$_4$** (**2**). The displacement ellipsoid plot is at the 50% probability level. Hydrogen atoms, lattice DMF and water molecules, and disorder have been omitted for clarity. Color scheme: light blue, dysprosium; green, manganese; yellow, sodium; red, oxygen; dark blue, nitrogen; and gray, carbon.

Figure 2. Single-crystal X-ray structure of {DyNa[12-MC$_{Mn(III)N(shi)}$-4]]}$_2$(dnic)$_4$(H$_2$O)$_{10}$·4DMF, **Dy$_2$Mn$_8$Na$_2$(dnic)$_4$** (**3**). The displacement ellipsoid plot is at the 50% probability level. Hydrogen atoms, lattice DMF molecules, and disorder have been omitted for clarity. Color scheme: light blue, dysprosium; green, manganese; yellow, sodium; red, oxygen; dark blue, nitrogen; and gray, carbon.
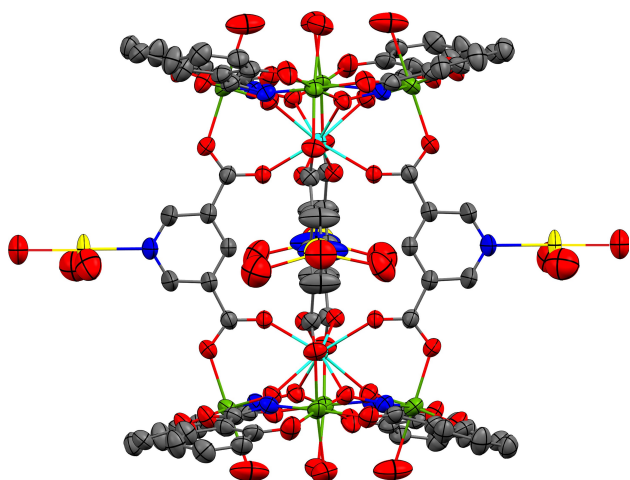

Figure 3. Single-crystal X-ray structure of [Hpy]$_2${Dy[12-MC$_{Ga(III)N(shi)}$-4]]}$_2$(dtba)$_4$(py)$_4$·2py·6MeOH, **Dy$_2$Ga$_8$(Hpy)$_2$(dtba)$_4$** (**5**). The displacement ellipsoid plot is at the 50% probability level. Hydrogen atoms, lattice pyridine and methanol molecules, and lattice pyridinium cations have been omitted for clarity. Color scheme: light blue, dysprosium; tan, gallium; yellow, sulfur; red, oxygen; dark blue, nitrogen; and gray, carbon.

Eur. J. Inorg. Chem. **2022**, e202200439 (4 of 14)

© 2022 Wiley-VCH GmbH

EurJIC
European Journal of Inorganic Chemistry

Research Article
doi.org/10.1002/ejic.202200439

Chemistry
Europe
European Chemical
Societies Publishing

Figure 4. Single-crystal X-ray structure of ; and {Ho[12-MC$_{Ga(III)N(shi)}$-4]}$_2$[Ga-(OH)(DMF)$_4$](dnic)$_4$(H$_2$O)(DMF)$_3$(py)$_2$·6DMF, **Ho$_2$Ga$_8$(Ga-OH)(dnic)$_4$ (7)**. In **7** only the metal centers of the MC and their first coordination environment were refined with anisotropic parameters. In the diagram, the displacement ellipsoids of these atoms are at the 50% probability level. Hydrogen atoms, lattice DMF molecules, and disorder have been omitted for clarity. Color scheme: light blue, holmium; tan, gallium; red, oxygen; dark blue, nitrogen; and gray, carbon.

the synthetic scheme for the compounds. In the presently reported structures the countercations are either Na$^+$, Hpy$^+$, or Ga^{III}, but in a series of related {Ln^{III}Na[12-MC$_{Ga(III)N(shi)}$-4]}$_2$(iph)$_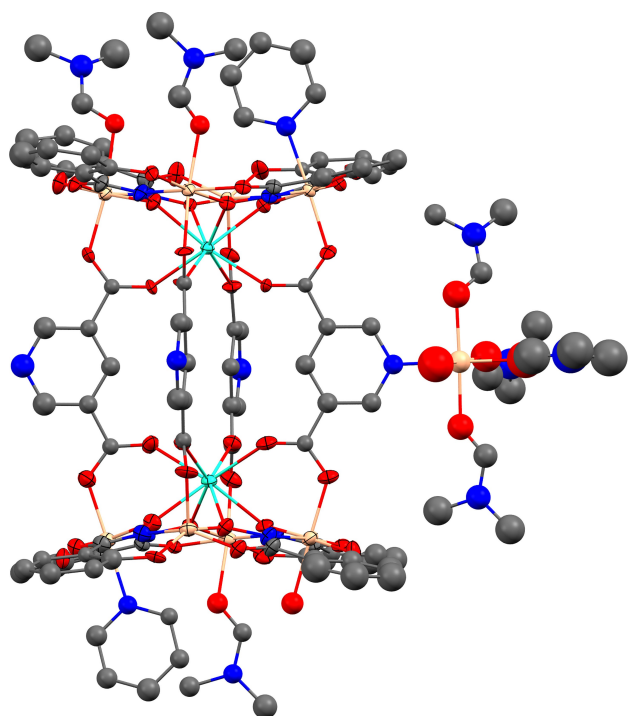4$ dimers (Ln=Y, Pr–Tm, except Pm), ammonium is utilized as the countercation.[21] Thus, the identity of the countercation is not vital to MC dimer formation and the dimer can accommodate a variety of species; however, the presence of a countercation is essential to the generation of the dimer. Lastly, oxidation states for the metal ions were evaluated based on overall molecular charge considerations and bond valence sum (BVS) values (Table S2).[32] In addition, each Mn^{III} ion of **1–3** possesses two axial bonds longer than the equatorial ones due to the Jahn-Teller distortion, which is consistent with a high spin 3d^4 electron configuration. We should note for **7** [**Ho$_2$Ga$_8$(Ga-OH)(dnic)$_4$**], which contains the peripheral Ga^{III} countercation, the BVS value for the peripheral gallium was 2.11 v.u. indicating a 2+ oxidation state. However, in the synthesis of the compound, gallium(III) nitrate hydrate was used as the starting material and no reducing agents were added to the reaction; thus, it is very unlikely the metal was reduced to 2+. The conflicting BVS value is likely due to the modeling of the coordination sphere about the peripheral gallium. Due to the amount of structural disorder about the coordination of the metal ion, it was difficult to establish exact bonding distances between the peripheral gallium and the solvent molecules. As

stated in the CIF, the DMF molecules are relatively mobile, and they were only refined with isotropic displacement parameters. The average bond distance for the peripheral gallium ion was 2.140 Å, while the average bond distances of the ring gallium ions of **7** ranged from 1.916 to 2.006 Å. This longer bond distance then leads to an assumption of a lower oxidation state in the BVS calculation, though from a chemical perspective a 2+ oxidation state is unrealistic.

Due to the large number of compounds, we will first succinctly describe the general similarities of the structural features. Then, we will mainly focus on the differences to facilitate a better understanding of the structures. For structures **1–7**, each central Ln^{III} ion is eight-coordinate, and a *SHAPE 2.1* analysis[33] (Table S3) reveals that the geometry for each Ln^{III} ion is best described as a square antiprism with continuous shape measurement (CShM) values all less than 1.0. CShM values less than 1.0 indicate that the geometry only has minimal distortions from the ideal shape.[33d] The [12-MC$_{M(III)N(shi)}$-4] framework is slightly domed, and the Ln^{III} ions are located on the convex side of each MC unit. The coordination sphere of each Ln^{III} is completed by four oxime oxygen atoms of the MC cavity and four carboxylate oxygen atoms of the dicarboxylate anion. Each carboxylate group then connects to a ring M^{III} ion via a three-atom bridge. The other carboxylate oxygen atom of the carboxylate group binds axially to the ring M^{III} ion. In addition, each Ln^{III} ion is linked to a ring M^{III} ion via a bridging oxime oxygen atom from the MC central cavity. For **1–3**, all of the ring Mn^{III} ions are six-coordinate with a distorted octahedral geometry (Table S4). The equatorial plane of each Mn^{III} consists of two *trans* shi^{3-} ligands. One shi^{3-} binds with an oxime oxygen atom and a carbonyl oxygen atom, while the other binds with an oxime nitrogen atom and a phenolate oxygen atom. The elongated axis consists of the aforementioned carboxylate oxygen atom of the dicarboxylate anion and of a solvent oxygen atom from either a water or DMF molecule. For **4** all of the Ga^{III} ions are six-coordinate with octahedral geometry (Table S4), while in **5–7**, each ring has a mixture of five- and six-coordinate Ga^{III} ions. The five-coordinate Ga^{III} ions have a spherical square pyramidal geometry (Table S5), and the six-coordinate Ga^{III} ions have an octahedral geometry. In all cases the equatorial plane of the Ga^{III} ions is the same as described for the Mn^{III} ions above, and, one of the axial ligands is a carboxylate oxygen atom from a dicarboxylate anion. For the six-coordinate Ga^{III} ions, the coordination is completed by a solvent molecule, either water (**4**, **6**, and **7**), DMF (**7**), and/or pyridine (**5**, **6**, and **7**). For the five-coordinate species, a solvent molecule is not bound to the Ga^{III} ion.

The main difference between the structures is due to the countercation. For **5** [**Dy$_2$Ga$_8$(Hpy)$_2$(dtba)$_4$**] and **6** [**Y$_2$Ga$_8$(Hpy)$_2$(dnic)$_4$**], two pyridinium cations that provide charge balance are located in the lattice. For **1**, **2**, and **4**, one sodium cation is bound to each central MC cavity, and they are located opposite of the central Ln^{III} ion. The sodium ions are located on the concave side of each MC unit. For **1** [**Dy$_2$Mn$_8$Na$_2$(iph)$_4$**] and **2** [**Dy$_2$Mn$_8$Na$_2$(tma)$_4$**] each sodium ion is eight-coordinate with the geometry best described as a biaugmented trigonal prism (Table S6). However, the geo-

Eur. J. Inorg. Chem. **2022**, e202200439 (5 of 14)

© 2022 Wiley-VCH GmbH

Chemistry Europe
European Chemical Societies Publishing

metries are considerably distorted as the CShM values are 3.306 and 3.760, respectively. Typically values over 3.0 indicate significant distortions from the ideal shape.[33d] The coordination sphere of the sodium ions is completed by four oxime oxygen atoms from the central MC cavity and four oxygens from water and/or DMF molecules. These oxygen atoms from the solvent molecules also bridge the sodium ion to each ring Mn^{III} ion. For **4 [Yb$_2$Ga$_8$Na$_2$(tma)$_4$]**, each central sodium ion is nine-coordinate with a spherical capped square antiprism geometry (Table S7). The coordination sphere contains four oxime oxygen atoms, four water molecules that bridge to the ring Ga^{III} ions, and a fifth water molecule that caps the cation. Both **2** and **4** contain the bridging ligand trimesate; however, the third carboxylate group of the ligand remains protonated and does not bind any metal ions. In **3 [Dy$_2$Mn$_8$Na$_2$(dnic)$_4$]** and **7 [Ho$_2$Ga$_8$(Ga-OH)(dnic)$_4$]**, the bridging ligand is dinicotinate, and in these structures the pyridyl nitrogen atom of the ligand does indeed bind a countercation. In **3** the sodium cations are disordered over the four dinicotinate ligands so that each sodium cation has a 0.5 occupancy. Each sodium cation is four-coordinate with square planar geometry (Table S8). The coordination sphere consists of the pyridyl nitrogen atom of the dinicotinate and oxygen atoms from three water molecules. In **7** a peripheral Ga^{III} ion binds to only one of the dinicotinate ligands and is not disordered over the other pyridyl nitrogen sites. The Ga^{III} ion is six-coordinate with octahedral geometry (Table S9). The coordination sphere is completed by a pyridyl nitrogen atom, four oxygen atoms from solvent DMF molecules, and an oxygen atom from a hydroxide anion.

Magnetic Properties

DC magnetometry

DC variable-magnetic field and variable temperature experiments were performed on the three Dy—Mn dimeric complexes **Dy$_2$Mn$_8$Na$_2$(iph)$_4$** (**1**), **Dy$_2$Mn$_8$Na$_2$(tma)$_4$** (**2**), and **Dy$_2$Mn$_8$Na$_2$(dnic)$_4$** (**3**) (Figure 5). They show similar magnetization curves from 0–7 T applied field at 2 K. A sharp curvature occurs from 0–2 T and a shallower increase in magnetization occurs from 2 T to higher fields. The magnetization for **Dy$_2$Mn$_8$Na$_2$(iph)$_4$**, **Dy$_2$Mn$_8$Na$_2$(tma)$_4$**, and **Dy$_2$Mn$_8$Na$_2$(dnic)$_4$** at 7 T is 15.70, 17.22, and 17.97 Nβ, respectively. Magnetic susceptibility from 2–300 K with a 2000 Oe applied field also show similar curvature for the three complexes, with sharp curvature below 100 K followed by a less pronounced increase in χ_MT from 100–300 K. The χ_MT values at 300 K are 56.55, 51.36, and 52.75 cm^{3}K mol^{-1} for **Dy$_2$Mn$_8$Na$_2$(iph)$_4$**, **Dy$_2$Mn$_8$Na$_2$(tma)$_4$**, and **Dy$_2$Mn$_8$Na$_2$(dnic)$_4$**, respectively.

AC susceptibility magnetometry

AC susceptibility measurements were performed on compounds **Dy$_2$Mn$_8$Na$_2$(iph)$_4$** (**1**), **Dy$_2$Mn$_8$Na$_2$(tma)$_4$** (**2**), and **Dy$_2$Mn$_8$Na$_2$(dnic)$_4$** (**3**) without an external magnetic field and
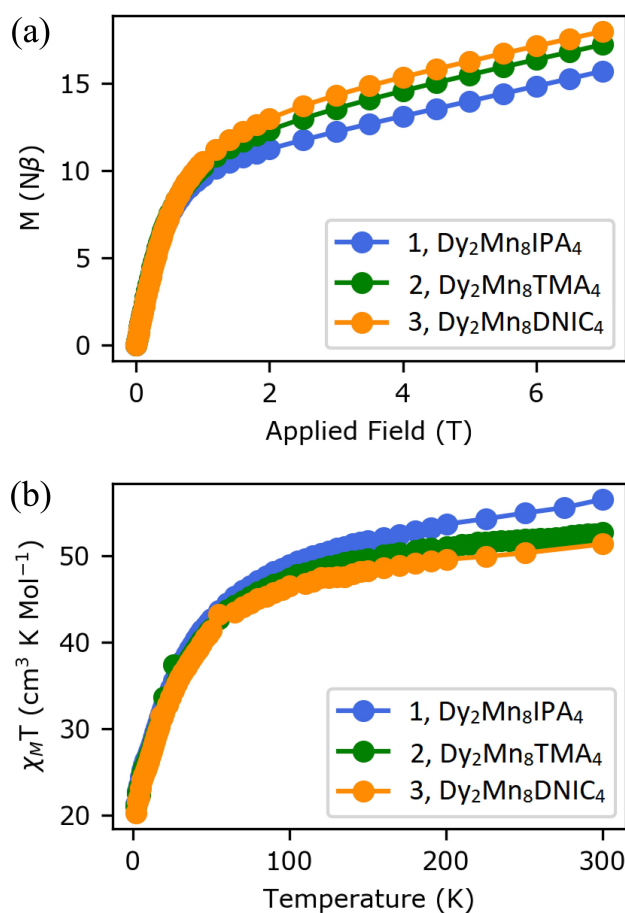
Figure 5. DC magnetometry for **Dy$_2$Mn$_8$Na$_2$(iph)$_4$** (**1**), **Dy$_2$Mn$_8$Na$_2$(tma)$_4$** (**2**), and **Dy$_2$Mn$_8$Na$_2$(dnic)$_4$** (**3**). (a) Powder DC magnetization at 2 K with an applied field from 0–7 T. (b) Powder magnetic susceptibility experiment from 2–300 K with an applied field of 2000 Oe (0.2 T). For complex **3**, three data points presumed overtly erroneous were omitted for clarity (Figure S4).

with a 3 Oe drive field while varying the temperature from 2–10 K and a varying drive field frequency of 10–1400 Hz (Figures S5–S7). All three complexes show similar out-of-phase molar AC susceptibility (χ_M'') behavior when plotted as χ_M'' versus drive field frequency, with an increase in χ_M'' as the field increased. However, in each case, the frequency dependence never peaked within our examined frequency and temperature range. The intensity of each peak decreased markedly as temperature increased, consistent with a shallow barrier to magnetic relaxation. The Cole-Cole plots (in-phase AC magnetic susceptibility versus out-of-phase AC magnetic susceptibility, χ_M' vs χ_M''; Figures S2–S4) are expected to show inverted parabolic shapes and can be fitted to glean information about spin relaxation dynamics. However, in each case insufficient curvature was present to fit the Cole-Cole plots because the χ_M'' peak occurred at higher frequencies than were experimentally accessible.

EurJIC
European Journal of Inorganic Chemistry

Research Article
doi.org/10.1002/ejic.202200439

Chemistry Europe
European Chemical
Societies Publishing

Structural Feature Comparison

From a multitude of structural measurements (Tables 1 and S10), it is apparent that the complexes are structurally very similar. Despite different central metal ions, ring metal ions, bridging ligands, and countercations (and their coordination mode), the dimeric metallacrowns of 1–4, 6, and 7 are nearly isostructural. The one exception is compound 5, [**Dy$_2$Ga$_8$(Hpy)$_2$(dtba)$_4$**], which contains the bridging ligand 2,2′-dithiodibenzoate. Due to the configuration of the dicarboxylate anion, structural variation is incorporated into the dimer, which we will discuss in detail below. For 1–4, 6, and 7, the greatest similarities are between structures that contain the same ring metal ions, either Mn^{III} (1–3) or Ga^{III} (4, 6, 7). Yet the overall differences between the Mn^{III}- and Ga^{III}-based structures are minimal. Each [12-MC$_{M(III)N(shi)}$-4] unit of the dimer is nearly identical in terms of the size of the MC cavity radius, the distance between adjacent metal centers, and the distance between adjacent oxime oxygen atoms. The corresponding distances do not vary more than 0.1 Å (Table 1). In addition, the presence or absence of the sodium countercation in the central cavity does not have a dramatic effect on the distance between the central Ln^{III} ion and the [12-MC$_{M(III)N(shi)}$-4] unit. For 1, 2, and 4 which contain a sodium ion in the MC central cavity, the Ln^{III}

ion resides slightly further from the ring metal mean plane and the oxime oxygen mean plane of the [12-MC$_{M(III)N(shi)}$-4] unit than in the structures without a central Na$^+$ (3, 5, 6, and 7), possibly due to Coulombic repulsion between the Ln^{III} and Na$^+$ ions. However, closer inspection of the Ln^{III}-mean plane distances indicates that the variability may be due to the differences in the geometries about the ring metal ions (Mn^{III} vs Ga^{III}) instead, which we discuss in more detail below.

In terms of the characteristics of the entire dimer for 1–4, 6, and 7, the use of different dicarboxylate anions and Ln^{III} ions does not lead to significant differences in the Ln–Ln distance across the dimer as the structural size of the bridging dicarboxylate anion does not significantly deviate. This is evident by measuring the average distance between the two carboxylate oxygen atoms of the same anion that bind opposite Ln^{III} ions. This distance does not deviate by more than 0.1 Å regardless of the identity of the central metal, ring metal, or dicarboxylate. However, there are differences in the axial direction of the dimer due to the ring metal identity. The Mn^{III} ions are high spin $3d^4$; thus, they possess an elongated Jahn-Teller axis. The average Mn^{III}-O$_{axial}$/N$_{axial}$ bond distances for 1–3 range from 2.25 to 2.30 Å, and the average Mn^{III}-O$_{carboxylate}$ bond distances range from 2.13 to 2.16 Å. However, Ga^{III} ions, due to their isotropic electron configuration, do not possess an

Table 1. Structural feature comparison of 1–7.[a]

	1	2	3	4	5		6	7	
MC Composition									
Central Metal[b]	Dy^{III}	Dy^{III}	Dy^{III}	Yb^{III}	Dy^{III}1	Dy^{III}2	Y^{III}	Ho^{III}1	Ho^{III}2
Ring Metal	Mn^{III}	Mn^{III}	Mn^{III}	Ga^{III}	Ga^{III}	Ga^{III}	Ga^{III}	Ga^{III}	
Countercation	Na$^+$ in central cavity	Na$^+$ in central cavity	Na$^+$ on periphery	Na$^+$ in central cavity	Hpy$^+$ in lattice		Hpy$^+$ in lattice	Ga^{III} on periphery	
Bridging Dicarboxylate	iph^{2-}	tma^{2-}	dnic^{2-}	tma^{2-}	dtba^{2-}		dnic^{2-}	dnic^{2-}	
Measurement									
Ln^{III} crystal radius (Å)	1.07	1.07	1.05	1.00	1.06	1.07	1.02	1.03	1.03
MC cavity radius (Å)	0.54	0.56	0.59	0.53	0.54	0.54	0.54	0.55	0.56
Avg. cross cavity O$_{ox}$-O$_{ox}$ distance (Å)	3.68	3.73	3.78	3.67	3.68	3.68	3.68	3.71	3.72
Avg. cross cavity O$_{carbLn}$-O$_{carbLn}$ distance (Å)	4.02	4.03	4.01	3.98	4.24	4.23	3.96	4.01	4.03
Ln^{III}-Ln^{III} distance (Å)	7.19	7.21	7.36	7.24	9.31		7.43	7.37	
Na–Na distance (Å)	14.34	14.48	11.61 (adj. Na) 16.42 (opp. Na)	14.12					
O$_{ox\ Centroid}$ - O$_{ox\ Centroid}$ distance (Å)	10.42	10.35	10.25	10.06	12.24		10.28	10.16	
O$_{carbLn}$-O$_{carbLn}$ distance (Å)	5.03	5.01	5.06	4.95	7.41		5.04	4.99	
O$_{carbMIII}$-O$_{carbMIII}$ distance (Å)	7.11	7.10	7.08	7.07	10.67		7.03	7.04	
Ln^{III}-Na distance (Å)	3.57	3.64	8.99	3.44					
Ln^{III}-O$_{ox}$MP distance (Å)	1.61	1.57	1.46	1.41	1.46	1.47	1.42	1.40	1.40
Ln^{III}-O$_{carbLn}$MP distance (Å)	1.08	1.10	1.15	1.14	1.08	1.08	1.20	1.19	1.19
Na-O$_{ox}$MP distance (Å)	1.96	2.07		2.03					
Avg. ring M^{III}-O$_{axial}$/N$_{axial}$ distance (Å)	2.30	2.28	2.25	2.13	2.03	2.02	2.07	2.08	2.06
Twist angle between opposite MC faces (°)[c]	0.08	0.00	0.00	0.00	87.37		0.18	0.33	

[a] Abbreviations: O$_{ox}$ – oxime oxygen atom of the MC ring, O$_{sol}$ – oxygen atom from either a solvent water or DMF molecule, O$_{carbLn}$ – the carboxylate oxygen atom of the dicarboxylate anion that is bound to the central Ln^{III} ion, O$_{carbMIII}$ – the carboxylate oxygen atom of the dicarboxylate anion that is bound to the ring M^{III} ion, O$_{axial}$/N$_{axial}$ – the oxygen or nitrogen atoms along the z-axis of the ring M^{III} ions, and MP – the mean plane for the four atoms specified. [b] For compounds 1–4 and 6, the lanthanide ions are related by an inversion center; thus, there is only one unique lanthanide per dimer. For 5 and 7, the lanthanide ions are not related by any symmetry elements; thus, each lanthanide ion and the corresponding [12-MC$_{M(III)N(shi)}$-4] unit is independent from the other. [c] The twist angle is between the ring M^{III} ions of opposite MC faces that share the same dicarboxylate anion and is defined as ring M^{III} – centroid of ring M^{III} of one MC – centroid of ring M^{III} of opposite MC – opposite ring M^{III}.

Eur. J. Inorg. Chem. **2022**, e202200439 (7 of 14)

© 2022 Wiley-VCH GmbH

EurJIC
European Journal of Inorganic Chemistry

Research Article
doi.org/10.1002/ejic.202200439

Chemistry Europe
European Chemical
Societies Publishing

elongated axis and the average Ga^{III}-O_{axial}/N_{axial} bond distances of **4**, **6**, and **7** range from 2.06 to 2.13 Å, and the average Ga^{III}-$O_{carboxylate}$ bond distances range from 1.97 to 2.00 Å. This difference in the axial bond lengths then leads to other structural differences, a few of which we will highlight here. For the Ga-dimers the distance between the centroids of the four Ga^{III} ions of each MC unit is ~0.3 Å shorter than the corresponding distance in the Mn-dimers. In addition, the Ln^{III} ions of the Ga-dimers can more closely approach the mean plane of the ring metals by ~0.2 Å compared to the Mn-dimers. This is also true of the Ln^{III}-oxime oxygen mean plane distance. The axial elongation about the Mn^{III} ions also affects the Ln^{III} geometry. In the Mn^{III}-dimers, the Ln^{III} resides closer to the mean plane of the carboxylate oxygen atoms from the dicarboxylate anion than to the mean plane of the oxime oxygen atoms by ~0.4 Å. While in the Ga-dimers, the Ln^{III} is more centered between the two planes as the Ln^{III} ion is only ~0.2 Å closer to the mean plane of the carboxylate oxygen atoms. In essence, the Jahn-Teller elongation of the Mn^{III} ions causes the Ln^{III} ion to reside closer the mean plane of the carboxylate oxygen atoms and further from the oxime oxygen metallacrown central cavity.

Overall, though, for **1–4**, **6**, and **7**, the dimers are remarkably similar regardless of differences in their structural components. This is a hallmark of metallacrown chemistry – the ability to make wholesale component substitutions without greatly affecting the overall structure. The largest variability to the structures though is introduced by incorporation the bridging anion 2,2'-dithiodibenzoate (**5**). This ligand is structurally differ-ent from the other dicarboxylate anions in two fundamental ways. First, it is longer as it contains two aromatic rings connected via a S–S bridge. For isophthalate, trimesate, and dinicotinate the average distance between the two carboxylate oxygen atoms of the same anion that bind opposite Ln^{III} ions ranges from 7.03 to 7.11 Å. For 2,2'-dithiodibenzoate, this same distance is 10.67 Å on average. This leads to the two [12-$MC_{M(III)N(shi)}$-4] ends of the dimer to be separated by a greater amount. In **1–4**, **6**, and **7** the Ln^{III}-Ln^{III} distance ranges from 7.19-7.43 Å, while in **5** the Ln^{III}-Ln^{III} distance is 9.31 Å. In addition, the distance between the centroids of the opposite ring oxime oxygen atoms for **1–4**, **6**, and **7** ranges from 10.06 to 10.42 Å, while in **5** the same distance is 12.24 Å. Secondly, the S–S bridge of the dicarboxylate introduces some flexibility into the bridging anion. For the other three bridges, the core of the dicarboxylate is a rigid aromatic ring. This rigidity leads to the dicarboxylate anion binding to ring metal centers that are exactly opposite of each other on each end of the dimer. For compounds **2**, **3**, and **4**, each dimer is centered about a crystallographic C_4 axis that is along the central cations of the dimer and there is an inversion center in the middle of the dicarboxylate anions; thus, the symmetry of the dimers dictates that the twist angle between the opposite metal centers is 0.00°. For **1** and **6** there is only an inversion center in the middle of the dicarboxylate anions, and for **7** the peripheral Ga^{III} ion breaks the symmetry of the dimer, thus the dimer only possesses a pseudo-C_4 axis. However, in all three cases the exact opposite metal centers are also nearly eclipsed with the twist

angles being 0.08° (**1**), 0.18° (**6**), and 0.33° (**7**). In **5** though the flexibility of the bridging ligand allows the ligand to bind metal centers that do not reside on exact opposite ends of the dimer. Instead the 2,2'-dithiodibenzoate contorts to bind to a ring metal that is adjacent to the exact opposite metal center. Thus, the ligand twists as it spans the dimer, and the average twist angle between metal centers that bind to the same 2,2'-dithiodibenzoate is 87.37°, indicating the metal centers are staggered relative to each other (Figure 6).

Though the use of 2,2'-dithiodibenzoate increases the distance between the [12-$MC_{M(III)N(shi)}$-4] units of the dimer, it does not significantly change the dimensions of the [12-$MC_{M(III)N(shi)}$-4] framework itself. The MC framework dimensions of **5** such as the distance between adjacent ring metal ions, the MC cavity radius, the cross cavity metal-metal distance, and the oxime-oxime cross cavity distance are very similar to the values of **1–4**, **6**, and **7** (Table 1). While the use of 2,2'-dithiodibenzoate leads to structural elongation of the dimer, the utilization of a bridging ligand with appropriately placed carboxylate groups demonstrates once again the utility of metallacrown complexes to form predictable structural motifs.

Magnetostructural Relationships

A quantitative analysis of the low temperature DC magnetic data for compounds **Dy₂Mn₈Na₂(iph)₄** (**1**), **Dy₂Mn₈Na₂(tma)₄** (**2**), and **Dy₂Mn₈Na₂(dnic)₄** (**3**) is quite complex because one needs to assess the exchange coupling interaction between the Dy^{III} and Mn^{III}, which is very weak. However, a qualitative description using data of related compounds where either Dy^{III} or Mn^{III} are replaced by diamagnetic ions can be performed. Dy^{III} has a $^6H_{15/2}$ ground multiplet with a Curie constant (C) = 14.2 cm^3 K mol^{-1}, while the Mn^{III} ions have an S = 2 spin state (C = 3 cm^3 K mol^{-1} with g = 2). The exchange coupling interac-tion in a previously reported compound, {Li[12-$MC_{Mn(III)N(shi)}$-4]}⁻ with Li^+ replacing the central Dy^{III} ion, shows a relatively weak antiferromagnetic coupling among the ring Mn^{III} ions within the metallacrown subunit with an exchange coupling parameter of J = −6.2 cm^{-1} ($H = -JS_i \cdot S_{i+1}$).[11] Since the exchange coupling between Dy^{III} and Mn^{III} is expected to be weaker, and the Dy^{III}-Dy^{III} exchange even weaker, at room temperature the χ_MT value is expected to be the sum of that of the individual ions (2 Dy^{III}x14.2 + 8 Mn^{III}x3 = 52.4 cm^3 K mol^{-1}), which corresponds to the value found for **2** and **3**, 51.36 and 52.75 cm^3 K mol^{-1}, respectively. The slightly larger value for **1** (56.55 cm^3 K mol^{-1}) is likely due to a slight error in the diamagnetism correction value especially given the amount disordered solvent molecules in the lattice.[29] Upon cooling down from room temperature, the χ_MT values decrease in a rate larger than that of mononuclear Dy^{III} complexes but similarly to the to the {Li[12-$MC_{Mn(III)N(shi)}$-4]}⁻ derivative, which is due to the antiferromagnetic coupling between the Mn^{III} ions within the MC subunits. At 2 K, the χ_MT reaches a value of ca. 19 cm^3 K mol^{-1}. This value is twice the one found in an already reported Dy₂Ga₄ complex where one Dy^{III} is replaced by the diamagnetic Y^{III} (yielding an isolated Dy^{III} center).[13] Thus, the susceptibility data are consistent with two
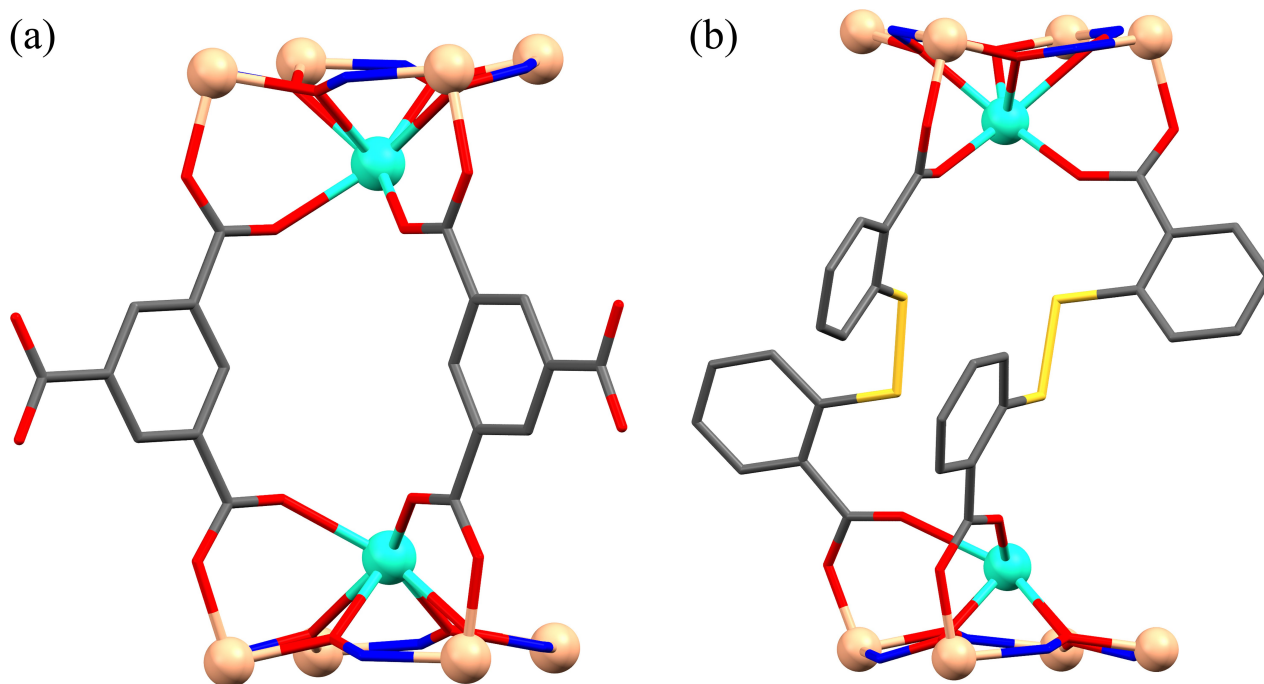
EurJIC
European Journal of Inorganic Chemistry

Research Article
doi.org/10.1002/ejic.202200439

Chemistry
Europe
European Chemical
Societies Publishing

Figure 6. Side-view of (a) **Yb$_2$Ga$_8$Na$_2$(tma)$_4$ (4)** and (b) **Dy$_2$Ga$_8$(Hpy)$_2$(dtba)$_4$ (5)** reduced to only the metallacrown ring atoms, the central lanthanide ions, and two of the four bridging dicarboxylate anions to emphasize the bonding motif of the bridging ligands. In both structures, the dicarboxylate anions are on neighboring Ga^{III} centers. In **4** the Ga^{III} centers connected by the same dicarboxylate are eclipsed, while **5** the Ga^{III} centers connected by the same dicarboxylate are staggered relative to each other by 87.37° on average. See previous figures for color scheme.

isolated Dy^{III} ions and two tetrameric Mn^{III} units, and the exchange coupling between the Dy^{III} and Mn^{III} ions is probably weaker than 2 K. For **1**–**3**, the magnetization increases sharply from 0 to 1 T where they reach a value of ca. 11 Nβ and increases in a linear fashion up to ca. 17 Nβ at 7 T without reaching saturation. The magnetization value at 1 T per DyMn$_4$ MC subunit (ca. 5.5 Nβ) is very close to that of the DyYGa$_4$ compound mentioned above where a value ca. 4.5 Nβ is reached at an applied field of 1 T that corresponds to the saturation value of that complex. The difference between the two magnetization values is likely due to the presence of the four antiferromagnetically coupled paramagnetic Mn^{III} ions as opposed to the four diamagnetic Ga^{III} ions. Here, the absence of saturation is probably due to the stabilization of the higher spin states (1, 2, 3 etc.) of the antiferromagnetically coupled four Mn^{III} ion belonging to the MC subunits that become more and more populated upon increasing the magnetic field. Again, the magnetic data are consistent with a sum of the magnetization of the Dy^{III} ions and those of the tetrameric Mn^{III} MC subunits. Moreover, a weak exchange coupling between Dy^{III} and Mn^{III} ions cannot be observed even when a large magnetic field is applied.

To examine for potential single-molecule magnet behavior, each Dy$_2$Mn$_8$ complex was analyzed via AC magnetometry (Figures S5–S7). In each case, out-of-phase magnetic susceptibility behavior was observed exhibiting a temperature and frequency dependence consistent with slow magnetic relaxation. However, the out-of-phase magnetic susceptibility did not peak within our experimental temperature/frequency range,

precluding extraction of the energy of the barrier to magnetic relaxation. The Cole-Cole plots, used to extract information about magnetic relaxation properties, similarly did not show adequate curvature to extract magnetic parameters.[34] In essence, the AC experiments suggest slow magnetic relaxation with a very small effective barrier to relaxation for the examined Dy$_2$Mn$_8$ complexes. Usually, for a Dy^{III} species with a square antiprism geometry and a strict four-fold symmetry axis as in the case of complexes **2**, **3**, and approximately **1**, the nature of the ground Kramers level and therefore the magnetic anisotropy can be analyzed qualitatively relying on the quadrupole approximation popularized by Rinehart and Long.[35] For Dy^{III}, an axial crystal field stabilizes large M_j values (typically ±15/2 or ±13/2), which corresponds to a high anisotropy barrier and favors SMM behavior. While an equatorial crystal field stabilizes small M_j values, which correspond to a rather planar anisotropy and therefore to a weak energy barrier. For [Dy^{III}Pc$_2$]$^-$, where Pc^{2-} is phthalocyaninato, the central Dy^{III} ion has a square antiprism geometry and a C$_4$ symmetry axis. The distance of the Dy^{III} ion from the two mean planes of nitrogen atoms of the Pc^{2-} cavity are 1.38 Å and 1.40 Å with an average Dy^{III}-N bond distance of 2.41 Å.[36] These structural features lead to a calculated ground level with $M_j = \pm 13/2$ favoring a rather large magnetic anisotropy and therefore a SMM behavior as observed experimentally for [Dy^{III}Pc$_2$]$^-$.[37] For **1**, **2** and **3**, the distance between the Dy^{III} and mean plane of oxime oxygen atoms of the MC cavity is 1.61, 1.57, and 1.46 Å, respectively, with an average Dy^{III}-O$_{ox}$ bond distance of 2.45, 2.44, and 2.39 Å, respectively, while the distance between the Dy^{III} and mean

EurJIC
European Journal of Inorganic Chemistry

Research Article
doi.org/10.1002/ejic.202200439

**Chemistry
Europe**
European Chemical
Societies Publishing

plane of carboxylate oxygen atoms of the dicarboxylate anions are shorter (1.08, 1.10, and 1.15 Å, respectively), with also shorter average $Dy^{III}-O_{carb}$ bond lengths (2.28, 2.30, and 2.31 Å, respectively). Thus, for $[Dy^{III}Pc_2]^-$ the Dy^{III} is better centered in the middle of the square antiprism, while for **1–3** the Dy^{III} is displaced closer to the carboxylate oxygen plane. Another important structural feature is the average bond angle produced by the adjacent carboxylate oxygen atoms about the coordination of the central Dy^{III} ($O_{carb}-Dy^{III}-O_{carb}$; **1**: 77.02°, **2**: 76.72°, **3**: 75.71°). These angles of the MCs are larger than the equivalent angle in the $[Dy^{III}Pc_2]^-$ structure. For $[DyPc_2]^-$ the average bond angle about the central Dy^{III} and the adjacent nitrogen atoms about the Pc^{2-} cavity ($N_{cavity}-Dy^{III}-N_{cavity}$) is 70.50°. Thus, the larger angles of **1–3** indicate that the crystal field about the Dy^{III} ion has much less axial character than for the Dy^{III} ion of $[DyPc_2]^-$. The less axial character and more equatorial crystal field of **1–3** likely stabilizes a ground state level with a smaller M_j value, which leads to a weaker magnetic anisotropy and, therefore, the lack of a SMM behavior above 2 K. The origin of this crystal field is probably both electronic as well as structural. The three dicarboxylate anions are rather strong bases that favor strong interaction with the Dy^{III} ions. [pK_a of parent acids - isophthalic acid: $pK_{a1} = 3.46$, $pK_{a2} = 4.46$, and $pK_a^{avg} = 3.96$; trimesic acid: $pK_{a1} = 3.12$, $pK_{a2} = 3.89$, and $pK_a^{avg} = 3.51$.[38]] More importantly, because the dicarboxylate anions bridge between Dy^{III} and Mn^{III} ions of one MC subunit and between two MC subunits, they impose a plane of oxygen atoms that favors planar magnetic anisotropy instead of an axial anisotropy.

As a final note, complex **$Dy_2Mn_8Na_2(iph)_4$** (**1**) was previously synthesized by Liu, Tong *et al.* though via a different synthetic route.[31] In their synthesis, the complex has the formula $\{DyNa[12-MC_{Mn(III)N(shi)}-4]\}_2(iph)_4(H_2O)_8 \cdot 18H_2O \cdot 10DMF$ and crystallized in the space group *I4/m*. While our compound has the formula $\{DyNa[12-MC_{Mn(III)N(shi)}-4]\}_2(iph)_4(H_2O)_2(DMF)_6 \cdot 6H_2O \cdot 4DMF$ and crystallizes in the space group $P\bar{1}$. Overall though the two structures are still quite similar with the same dimeric structure. Besides the difference in the amount of solvent in the lattice, the Liu, Tong *et al.* compound only has water molecules bridging between the ring Mn^{III} ions and the central Na^+ ion; while, in our structure there is a mixture of water and DMF molecules that bridge the two metal ions. In addition, the magnetic susceptibility curve shapes are similar as well; however, our complex **1** reached a $\chi_M T$ value of 56.6 $cm^3\,K\,mol^{-1}$ at 300 K (2000 Oe field) while the previous group measured 47.5 $cm^3\,K\,mol^{-1}$ at 300 K (1000 Oe field). At 2 K the magnetization value of the Liu, Tong *et al.* compound is 14.75 Nβ at 7 T, which is comparable to our value of 15.70 Nβ at 7 T. Curiously, the Liu, Tong *et al.* complex did not display slow relaxation of the magnetization. It is possible that a difference in solvation level of the solid leads to these discrepancies, but at the present time we do not have a conclusive explanation for the different AC magnetic susceptibility behavior.

Conclusion

A series of Ln_2M_8 ($Ln^{III} = Dy$, Ho, Yb, or Y and $M^{III} = Mn$ or Ga) dimer metallacrowns, $\{Ln[12-MC_{M(III)N(shi)}-4]\}_2$, were synthesized with varying bridging ligands and countercations to analyze the effect of these substitutions on the structural features of the dimers and on the magnetic behavior of the Dy_2Mn_8 dimers. For the investigated dimers with the bridging dicarboxylate anions isophthalate, trimesate, and dinicotinate, the identity of the bridging ligand and the identity or placement of the counter-cation (Na^+, pyridinium, or Ga^{III}) lead to only subtle changes in the structure of the dimer with little effect on the [12-$MC_{M(III)N(shi)}$-4] framework. Though structural changes, in particular the distance of the central Ln^{III} ion from the ring metal mean plane and oxime oxygen mean plane, were observed between the dimers with either manganese or gallium ions in the ring positions of the metallacrown. For the Mn-dimers, the Ln^{III} ions were further from these mean planes likely due to the elongated Jahn-Teller axis of each high spin $3d^4$ Mn^{III} ion. One of the axial ligands of the Mn^{III} ions is a carboxylate oxygen atom of the bridging dicarboxylate ligand and this carboxylate group also bridges between the ring Mn^{III} and the central Ln^{III} ions. Since the carboxylate group is further from the mean planes in the Mn-based dimers, the Ln^{III} is consequently pulled further from the mean planes. The ring Ga^{III} ions do not possess an elongated axis along this same direction due to the isotropic electron configuration and accordingly the Ln^{III} ions of these structures more closely approach the metal and oxime oxygen mean planes. Significant structural changes were only noted for the dimer with the bridging ligand 2,2'-dithiodiben-zoate as this ligand is longer and more flexible than the other dicarboxylate anions. The structural differences of 2,2'-dithiodi-benzoate leads to a longer dimer as evident in greater Ln–Ln distances compared to the other structures. Lastly, the use of 2,2'-dithiodibenzoate leads to the potential to bind a metal ion within the formed S_8 cavity between the two Ln^{III} ions to yield a MS_8 coordination environment.

In addition, the structures showcased how countercations can be bound to the MC dimer. For the structures **$Dy_2Mn_8Na_2(iph)_4$** (**1**), **$Dy_2Mn_8Na_2(tma)_4$** (**2**), and **$Yb_2Ga_8Na_2(tma)_4$** (**4**), a sodium cation is captured in each central cavity opposite to that of the Ln^{III} ion. However, for two of the dimers with dinicotinate, **$Dy_2Mn_8Na_2(dnic)_4$** (**3**) and **$Ho_2Ga_8(Ga-OH)(dnic)_4$** (**7**), the counter cation Na^+ or Ga^{III} binds to the pyridyl nitrogen of the bridging ligand. These examples demonstrate that it is possible to decorate the dimer with other metal ions. Though network formation is not achieved in the present cases as the coordination sphere of the Na^+ and Ga^{III} ions are completed with solvent molecules, one could envision using this position for metal binding that then could lead to higher dimensional structures by linking together MC dimers. Another possibility would be to attach paramagnetic metal centers at this pyridyl position and perhaps enhancing the magnetic properties of the dimers. Moreover, the dimers with trimesate could also be used in a similar manner. In the presented structures, the third carboxylic acid group remains protonated. If this group could be deprotonated in the

Eur. J. Inorg. Chem. **2022**, e202200439 (10 of 14)

© 2022 Wiley-VCH GmbH

EurJIC
European Journal of Inorganic Chemistry

Research Article
doi.org/10.1002/ejic.202200439

Chemistry Europe
European Chemical
Societies Publishing

presence of an appropriate templating metal, network formation and multidimensional materials could result, or paramagnetic metal ions could be attached to the deprotonated functional group. Furthermore, one might also imagine functionalizing the dimer at this free carboxylic acid group through reactions such as esterification, thioesterification, amidation, or acid anhydride condensation. This would represent a means to functionalize an already formed metallacrown.

The magnetic properties of the dimers $Dy_2Mn_8Na_2(iph)_4$ (**1**), $Dy_2Mn_8Na_2(tma)_4$ (**2**), and $Dy_2Mn_8Na_2(dnic)_4$ (**3**) were investigated by magnetization and DC and AC magnetic susceptibility experiments. All three complexes displayed similar DC magnetic behavior suggesting antiferromagnetic coupling between the ring Mn^{III} ions with each other. In addition, all three complexes showed slow relaxation of the magnetization consistent with a very small energy barrier.

Experimental Section

Materials

Manganese(II) nitrate tetrahydrate (98%) and dysprosium nitrate pentahydrate (99.9%) were purchased from Alfa Aesar. Salicylhydroxamic acid (>98.0%) and thiosalicylic acid (≥90.0%) were purchased from TCI America. Gallium nitrate hydrate (99.9%), yttrium nitrate hexahydrate (99.8%), holmium nitrate pentahydrate (99.9%), ytterbium nitrate pentahydrate (99.9%), 3,5-pyridinedicarboxylic (dinicotinic) acid (98%), trimesic acid (95%), pyridine (>99%), and diethyl ether (>99%) were purchased from Sigma-Aldrich. Sodium hydroxide (Certified ACS grade) and potassium hydroxide (ca. 85%; ACS grade) were purchased from Fisher Scientific. *N,N*-Dimethylformamide (DMF, ACS grade) was purchased from VWR Chemicals BDH. All reagents were used as received without further purification. All reactions were carried out aerobically under ambient conditions.

Syntheses

1, {DyNa[12-MC$_{Mn(III)N(shi)}$-4]}$_2$(iph)$_4$(H$_2$O)$_2$(DMF)$_6$·6H$_2$O·4DMF, **Dy$_2$Mn$_8$Na$_2$(iph)$_4$**. The synthesis and crystal structure of this compound have been previously reported.[29] ESI-MS, calculated for $[M]^{2-}$, Dy$_2$Mn$_8$C$_{88}$H$_{48}$N$_8$O$_{40}$, 1310.8; found, 1310.3. Elemental analysis for Dy$_2$Na$_2$Mn$_8$C$_{118}$H$_{134}$N$_{18}$O$_{58}$ (FW = 3542.90 g/mol): Calculated (%) C = 40.00, H = 3.81, N = 7.12; Found (%) C = 40.01, H = 3.62, N = 7.13.

2, {DyNa[12-MC$_{Mn(III)N(shi)}$-4]}$_2$(tma)$_4$(H$_2$O)$_8$·5H$_2$O·14DMF, **Dy$_2$Mn$_8$Na$_2$(tma)$_4$**. Dysprosium nitrate pentahydrate (0.125 mmol, 0.0548 g) and manganese nitrate tetrahydrate (0.5 mmol, 0.1255 g) were dissolved in 5 mL of DMF resulting in a clear and colorless solution. In a separate flask, salicylhydroxamic acid (0.5 mmol, 0.0766 g), trimesic acid (0.25 mmol, 0.0525 g), and sodium hydroxide (1.5 mmol, 0.0600 g) were dissolved in 5 mL of dimethylformamide resulting in a clear and colorless solution. The two solutions were mixed together and initially forming a clear and colorless solution. The solution was stirred overnight resulting in a green-brown solution. Then the solution was filtered via gravity filtration, yielding a dark brown filtrate and yellow-green precipitate. The precipitate was discarded, and the filtrate was set for slow evaporation which yielded black cubic crystals after 10 days. Yield: 4%. ESI-MS, calculated for $[M]^{2-}$, Dy$_2$Mn$_8$C$_{92}$H$_{48}$N$_8$O$_{48}$, 1398.8; found, 1398.3. Elemental analysis for Dy$_2$Na$_2$Mn$_8$C$_{134}$H$_{172}$N$_{22}$O$_{75}$ (FW = 4101.39 g/

mol): Calculated (%) C = 39.24, H = 4.23, N = 7.51; Found (%) C = 38.56, H = 4.35, N = 7.25.

3, {DyNa[12-MC$_{Mn(III)N(shi)}$-4]}$_2$(dnic)$_4$(H$_2$O)$_{10}$·4DMF, **Dy$_2$Mn$_8$Na$_2$(dnic)$_4$**. Dysprosium nitrate pentahydrate (0.125 mmol, 0.0548 g), manganese nitrate tetrahydrate (0.5 mmol, 0.1255 g), salicylhydroxamic acid (0.5 mmol, 0.0766 g), and dinicotinic acid (0.25 mmol, 0.0418 g) were dissolved in 20 mL of DMF resulting in a clear and colorless solution. A concentrated solution of aqueous sodium hydroxide (~19.8 M) was added (2.0 mmol, 101 μL) and the mixture turned brown in color. After stirring overnight, the solution was gravity filtered to yield a green-brown filtrate and yellow-green precipitate. The precipitate was discarded while the filtrate was set for slow evaporation. Green-black plate-like crystals were collected after two weeks. Yield: 7%. ESI-MS, calculated for $[M]^{2-}$, Dy$_2$Mn$_8$C$_{84}$H$_{44}$N$_{12}$O$_{40}$, 1312.8; found, 1312.3. Elemental analysis for Dy$_2$Na$_2$Mn$_8$C$_{96}$H$_{92}$N$_{16}$O$_{54}$ (FW = 3144.32 g/mol): Calculated (%) C = 36.67, H = 2.95, N = 7.13; Found (%) C = 36.80, H = 3.42, N = 7.60.

4, {YbNa[12-MC$_{Ga(III)N(shi)}$-4]}$_2$(tma)$_4$(H$_2$O)$_{10}$·3H$_2$O·15DMF, **Yb$_2$Ga$_8$Na$_2$(tma)$_4$**. Ytterbium nitrate pentahydrate (0.25 mmol, 0.1123 g), gallium nitrate hydrate (1.0 mmol, 0.3638 g), salicylhydroxamic acid (1.0 mmol, 0.1531 g), and trimesic acid (0.5 mmol, 0.1051 g) were dissolved in 30 mL of DMF resulting in a clear and colorless solution. A concentrated solution of aqueous sodium hydroxide (~19.8 M) was added (4.0 mmol, 202 μL). The mixture was stirred for three hours, then the stirring was stopped, and the mixture was allowed to sit undisturbed overnight. The next day, the mixture was gravity filtered and the clear and colorless filtrate was set to crystallize, producing crystalline material after about one week. Yield: 10%. ESI-MS, calculated for $[M]^{2-}$, C$_{92}$H$_{48}$Yb$_2$Ga$_8$N$_8$O$_{48}$, 1468.7; found, 1468.5. Elemental Analysis for C$_{137}$H$_{179}$Yb$_2$Ga$_8$N$_{23}$Na$_2$O$_{76}$ (FW = 4313.84 g/mol): Calculated (%) C = 38.14, H = 4.18, N = 7.47; Found (%) C = 38.07, H = 4.22, N = 7.54.

5, [Hpy]$_2${Dy[12-MC$_{Ga(III)N(shi)}$-4]}$_2$(dtba)$_4$(py)$_4$·2py·6MeOH, **Dy$_2$Ga$_8$(Hpy)$_2$(dtba)$_4$**. Dysprosium nitrate pentahydrate (0.0625 mmol, 0.0274 g), gallium nitrate hydrate (0.25 mmol, 0.0910 g), and salicylhydroxamic acid (0.25 mmol, 0.0383 g) were dissolved in 30 mL of methanol. Then potassium hydroxide (85%; 1.0 mmol, 0.0660 g) was added, and the mixture was stirred for 10 minutes. Following, thiosalicylic acid (0.25 mmol, 0.0385 g) was added, and the mixture was stirred overnight. The following morning 5 mL of pyridine were added, and then the mixture was stirred for 5 minutes. Then the mixture was allowed to sit for several hours before being gravity filtered. The filtrate was left to slowly evaporate, and a small number of colorless crystals were collected after two weeks. The crystals were analyzed by X-ray diffraction.

In an effort to collect more material several attempts were made to synthesize the compound again; however, the procedure is difficult to routinely reproduce. On other attempts, after 1 week of slow evaporation of the solvent, the mother liquor (~1 mL) was transferred to a new vial leaving behind colorless crystals of salt (presumably KNO$_3$). After an additional two weeks, a powder developed which was redissolved in ~3 mL of pyridine and ~4 mL of methanol. The solution was then gravity filtered to yield a clear, yellow solution. This solution was then reduced to ~1 mL by a stream of nitrogen gas. The vial was capped with a pinpricked foil lid and set for vapor diffusion with diethyl ether. A small amount of microcrystalline solid (0.3% yield) was obtained along with amorphous powder after one day. The crystals were analyzed by ESI-MS: calculated for $[M]^{2-}$, Dy$_2$Ga$_8$C$_{112}$H$_{64}$N$_8$O$_{40}$S$_8$, 1650.7; found 1650.7.

6, [Hpy]$_2${Y[12-MC$_{Ga(III)N(shi)}$-4]}$_2$(dnic)$_4$(py)$_6$·4DMF, **Y$_2$Ga$_8$(Hpy)$_2$(dnic)$_4$**. Salicylhydroxamic acid (1.0 mmol, 0.1531 g) was dissolved in 8 mL of DMF. Pyridine (1 mL), yttrium nitrate pentahydrate (0.3 mmol,

Eur. J. Inorg. Chem. **2022**, e202200439 (11 of 14)

© 2022 Wiley-VCH GmbH

0.1095 g), gallium nitrate hydrate (1.0 mmol, 0.3638 g), and dinicotinic acid (0.6 mmol, 0.1003 g) were added, resulting in a clear and colorless solution. The mixture was stirred for two hours, then was allowed to rest for two hours and the precipitate filtered out. Aliquots of 2 mL of the resulting clear solution were placed into vials, and the compound left to crystallize by diethyl ether vapor diffusion. Colorless crystals were collected after three weeks. Yield: 8%. ESI-MS, calculated for $[M]^{2-}$, $C_{84}H_{44}Y_2Ga_8N_{12}O_{40}$, 1298.5; found, 1298.7. Elemental analysis for $C_{136}H_{114}Y_2Ga_8N_{24}O_{44}$ (FW = 3524.09 g/mol): Calculated (%) C = 46.35, H = 3.26, N = 9.54; Found (%) C = 46.42, H = 3.13, N = 9.43.

7, $\{Ho[12\text{-}MC_{Ga(III)N(shi)}\text{-}4]\}_2[Ga(OH)(DMF)_4](dnic)_4(H_2O)(DMF)_3(py)_2 \cdot 6DMF$, **$Ho_2Ga_8(Ga\text{-}OH)(dnic)_4$**. Salicylhydroxamic acid (1.0 mmol, 0.1531 g) was dissolved in 8 mL of DMF. Pyridine (1 mL), holmium nitrate pentahydrate (0.3 mmol, 0.1323 g), gallium nitrate hydrate (1.1 mmol, 0.4002 g), and dinicotinic acid (0.5 mmol, 0.0836 g) were added, resulting in a clear and colorless solution. The mixture was stirred for two hours, then was allowed to rest for two hours and the precipitate filtered out. Aliquots of 2 mL of the resulting clear solution were placed into vials, and the compound left to crystallize by diethyl ether vapor diffusion. Colorless crystals were collected after three weeks. Yield: 6%. ESI-MS, calculated for $[M]^{2-}$, $C_{84}H_{44}Ho_2Ga_8N_{12}O_{40}$, 1374.5; found, 1374.7. Elemental analysis for $C_{133}H_{148}Ho_2Ga_9N_{27}O_{55}$ (FW = 3962.11 g/mol): Calculated (%): C = 40.32, H = 3.77, N = 9.54; Found (%) C = 40.26, H = 3.68, N = 9.30.

Physical Methods

Mass spectrometry. Electrospray ionization mass spectrometry (ESI-MS) spectra for **1**–**5** were collected with an Agilent 6230 TOF HPLC-MS mass spectrometer in negative ion mode (−350 V) on samples dissolved in methanol at a concentration of 0.5 mg/mL. ESI-MS spectra for **6** and **7** (dissolved in methanol) were collected on a Micromass LCT TOF electrospray ionization mass spectrometer, using a capillary voltage of 3500 V and a desolvation temperature of 350 °C. Samples (40 μM) were injected through direct infusion using a syringe pump at 11 μL/min, and the spectra were recorded in full scan analysis mode in the range m/z 100–2000.

Elemental analysis. Analyses for **1**–**5** were performed by Atlantic Microlabs Inc, Norcross, Georgia, United States. Analyses for **6** and **7** were performed at the University of Parma using a Thermo Fisher FlashSmart elemental analyzer.

X-ray crystallography. Crystals of **1** and **2** used for single crystal X-ray diffraction were taken from the mother liquor and were not dried. A mineral oil coated crystal was mounted on a MicroMesh MiTeGen micromount and transferred to the diffractometer. The data were collected on a Bruker AXS D8 Quest diffractometer equipped with a solid state CMOS area detector and a fine focus sealed tube X-ray source using Mo Kα radiation (λ = 0.71073 Å) monochromated with a Triumph curved graphite crystal. All data were collected at 150 K, and data collection and cell refinement was performed using APEX3 (version 2018.1-0) and SAINT embedded in APEX3, respectively.[39] The data were scaled and corrected for absorption with SADABS as built into APEX3.[39,40] Space groups were assigned using XPREP.[41] The structures were solved using direct methods with SHELXS-97 and refined using least-squares refinements based on F^2 with SHELXL-2018/3 and the graphical interface SHELXLE.[42–44] For **2** the structure contains four additional independent solvent accessible voids of 2885 Å³ combined (approximately 28% of the unit cell volume). The residual electron density peaks were not arranged in an interpretable pattern. The structure factors were instead augmented via reverse Fourier transform methods using the SQUEEZE routine as implemented in the program PLATON.[45,46] The resultant FAB file

containing the structure factor contribution from the electron content of the void space was used in together with the original hkl file in the further refinement. The FAB file with details of the Squeeze results is appended to the CIF file. The Squeeze procedure corrected for 564 electrons within the solvent accessible voids belonging to most likely extensively disordered methanol molecules.

Crystals of **3** and **5** were mounted on a Rigaku AFC10 K Saturn 944+ CCD-based X-ray diffractometer equipped with a low temperature device and Micromax-007HF Cu-target micro-focus rotating anode (λ = 1.54187 Å) operated at 1.2 kW power (40 kV, 30 mA). Rigaku d*trek images were exported to CrysAlisPro for processing and corrected for absorption. Analysis of the data showed negligible decay during data collection. The structure was solved and refined with the Bruker SHELXTL (version 2018/3) software package.[43] Non-hydrogen atoms were refined anisotropically with the hydrogen atoms placed in a combination of idealized and refined positions. For **3** and **5** the SQUEEZE subroutine of the PLATON program suite was used to address the disordered solvent contained in solvent accessible voids present in the structure.[46,47] The FAB files with details of the Squeeze results are appended to the CIF files. For **3** and **5**, the structures contain solvent accessible voids of 5227 Å³ and 1805 Å³, respectively. The Squeeze procedure corrected for 1370 electrons for **3** and 408 electrons for **5** within the solvent accessible voids belonging to most likely extensively disordered solvent molecules.

Colorless blocks of **4** were taken from solution and not dried. X-ray diffraction data for compound **4** was collected using a VENTURE PHOTON100 CMOS Bruker diffractometer with a Cu Kα radiation micro-focus IuS source. The crystal was mounted on a CryoLoop (Hampton Research) with Paratone-N (Hampton Research) as cryoprotectant and then flashfrozen in a nitrogen-gas stream at 100 K. The temperature of the crystal was maintained at 100 K by means of a 700+ series Cryostream cooling device to within an accuracy of ±1 K. The data were corrected for Lorentz polarization, and absorption effects. The structures were solved by direct methods using SHELXS-97 and refined against F^2 by full-matrix least-squares techniques using SHELXL-2018[42] with anisotropic displacement parameters for all non-hydrogen atoms. Hydrogen atoms were located on a difference Fourier map and introduced into the calculations as a riding model with isotropic thermal parameters. All calculations were performed by using the Crystal Structure crystallographic software package WINGX.[48]

Single crystal X-ray diffraction data of **6** were collected at the X-ray diffraction beamline (XRD1) of the Elettra Synchrotron, Trieste (Italy).[49] Crystals were dipped in NHV oil (Jena Bioscience GmbH) and mounted on the goniometer head with a nylon loop. Datasets were collected at 100 K (nitrogen stream supplied through an Oxford Cryostream 700) through the rotating crystal method. Data were acquired using a monochromatic wavelength of 0.700 Å on a *Pilatus 2 M* hybrid-pixel area detector. The diffraction data were indexed and integrated using XDS.[50] Scaling was done using the CCP4-Aimless code.[51] The structures were solved using SHELXT.[43] Fourier analysis and refinement were performed by the full-matrix least-squares method based on F^2 implemented in SHELXL-2014. Single crystal data for **7** were collected with a *Bruker Smart* diffractometer equipped with an *APEXII* CCD at 215 K, Mo Kα: λ = 0.71073 Å. The intensity data were integrated from several series of exposures frames (0.3° width) covering the sphere of reciprocal space. Data collection and cell refinement were performed using APEX3 and SAINT embedded in APEX3, respectively.[39] Absorption correction were applied using the program SADABS.[40] Compound **6** and **7** exhibit significant disorder in the main molecular fragment. Two orientations were clearly identified from the electron density maps, and they were refined with approximately 0.8/0.2 site

Eur. J. Inorg. Chem. **2022**, e202200439 (12 of 14)

© 2022 Wiley-VCH GmbH

EurJIC
European Journal of Inorganic Chemistry

Research Article
doi.org/10.1002/ejic.202200439

Chemistry Europe
European Chemical
Societies Publishing

occupancy factors. In particular, for the minor orientation, the heavy atoms, the coordination environment and some of the C atoms of the phenyl rings could be located from the difference map. For both systems, the minor orientation was therefore refined, by taking into account the molecular fragment of the major image, which was rotated and fitted to the residual density peaks. Several constraints and restraints were applied on both molecular fragments. In **6**, the minor orientation, and the solvent molecules of coordination and of crystallization were refined with isotropic thermal parameters. In **7**, only the metal centers of the metallacrown and their coordination environment were refined with anisotropic thermal parameters. In **6** and **7**, some portion of the lattice contained solvent accessible voids, which were modelled with the mask procedure implemented in Olex2.[52]

For compounds **1**–**7**, additional crystallographic data, refinement details, and experimental parameters are provided in the Supplementary Information, Table S1, and the individual CIFs of each compound.

Magnetic measurements. Magnetic measurements for **1**–**3** were performed using a Quantum Design MPMS X L7 SQUID magnetometer. Samples were homogenized by grinding with a mortar and pestle, then placed in a gelatin capsule with a small amount of melted eicosane. The eicosane was allowed to solidify to prevent the sample from torqueing at high fields. Variable field DC measurements were performed at 2 K with fields ranging from 0–7 T. Variable temperature DC measurements were performed from 2–300 K with a 0.2 T applied field. Diamagnetic corrections were applied to DC data based on Pascal's constants. AC magnetic susceptibility experiments were performed without an external magnetic field and from 2–10 K in 0.5 K increments with a 3 Oe $(3\times10^{-4}$ T) drive magnetic field oscillating from 10–1400 Hz in 16 even log-scale steps.

Data availability

Experimental procedures and details, additional crystallographic refinement details, crystallographic data, bond valence sum values, continuous shape measurement values, structural measurements, crystallographic figures, and magnetic data can be found in the Supporting Information.

Deposition Numbers 2030729 (for **1**), 2163142 (for **2**), 2163140 (for **3**), 2163143 (for **4**), 2163145 (for **5**), 2163141 (for **6**), and 2163144 (for **7**) contain the supplementary crystallographic data for this paper. These data are provided free of charge by the joint Cambridge Crystallographic Data Centre and Fachinformationszentrum Karlsruhe Access Structures service www.ccdc.cam.ac.uk/structures.

Author contributions

E. V. Salerno: Data curation, formal analysis, investigation, writing – original draft and review & editing. C. M. Foley: Investigation and writing – review & editing. V. Marzaroli: Investigation. B. L. Schneider: Investigation and writing – review & editing. M. D. Sharin: Investigation. J. W. Kampf: Data curation, formal analysis, funding acquisition, and writing –review & editing. L. Marchiò: Data curation, formal analysis, funding acquisition, and writing – review & editing. M. Zeller: Data curation, formal analysis, funding acquisition, and writing – review & editing. R. Guillot: Data curation, formal analysis, and writing – review & editing. T. Mallah: Conceptualization, formal analysis, funding acquisition, supervision, and writing – review & editing. M. Tegoni: Conceptualization, formal analysis, funding acquisition, supervision, and writing – review & editing. C. M. Zaleski: Conceptualization, formal analysis, funding acquisition, supervision, and writing – original draft and review & editing. V. L. Pecoraro: Conceptualization, formal analysis, funding acquisition, supervision, and writing – review & editing.

Conflict of Interest

This project uses intellectual property invented by Dr. Vincent Pecoraro at the University of Michigan that is under negotiation for license to VIEWaves. Dr. Pecoraro is a co-founder with equity interests in VIEWaves. The other authors have no conflicts to declare.

Data Availability Statement

The data that support the findings of this study are available in the supplementary material of this article.

[1] C. H. Hendon, A. J. Rieth, M. D. Korzyński, M. Dincă, *ACS Cent. Sci.* **2017**, *3*, 554–563.
[2] C. Pu, H. Qin, Y. Gao, J. Zhou, P. Wang, X. Peng, *J. Am. Chem. Soc.* **2017**, *139*, 3302–3311.

Eur. J. Inorg. Chem. **2022**, e202200439 (13 of 14)

© 2022 Wiley-VCH GmbH

[3] M. P. U. Haris, R. Bakthavatsalam, S. Shaikh, B. P. Kore, D. Moghe, R. G. Gonnade, D. D. Sarma, D. Kabra, J. Kundu, *Inorg. Chem.* **2018**, *57*, 13443–13452.

[4] J. Li, P. I. Djurovich, B. D. Alleyne, M. Yousufuddin, N. N. Ho, J. C. Thomas, J. C. Peters, R. Bau, M. E. Thompson, *Inorg. Chem.* **2005**, *44*, 1713–1727.

[5] M. Ostrowska, I. O. Fritsky, E. Gumienna-Kontecka, A. V. Pavlishchuk, *Coord. Chem. Rev.* **2016**, *327–328*, 304–332.

[6] a) M. S. Lah, V. L. Pecoraro, *Comments Inorg. Chem.* **1990**, *11*, 59–84; b) G. Mezei, C. M. Zaleski, V. L. Pecoraro, *Chem. Rev.* **2007**, *107*, 4933–5003.

[7] J. J. Bodwin, A. D. Cutland, R. G. Malkani, V. L. Pecoraro, *Coord. Chem. Rev.* **2001**, *216–217*, 489–512.

[8] C. Y. Chow, R. Guillot, E. Rivière, J. W. Kampf, T. Mallah, V. L. Pecoraro, *Inorg. Chem.* **2016**, *55*, 10238–10247.

[9] T. T. Boron III, J. C. Lutter, C. I. Daly, C. Y. Chow, A. H. Davis, R. Nimthong, M. Zeller, J. W. Kampf, C. M. Zaleski, V. L. Pecoraro, *Inorg. Chem.* **2016**, *55*, 10597–10607.

[10] C. M. Zaleski, J. W. Kampf, T. Mallah, M. L. Kirk, V. L. Pecoraro, *Inorg. Chem.* **2007**, *45*, 1954–1956.

[11] C. M. Zaleski, S. Tricard, E. C. Depperman, W. Wernsdorfer, T. Mallah, M. L. Kirk, V. L. Pecoraro, *Inorg. Chem.* **2011**, *50*, 11348–11352.

[12] C. M. Zaleski, E. C. Depperman, J. W. Kampf, M. L. Kirk, V. L. Pecoraro, *Angew. Chem. Int. Ed.* **2004**, *43*, 3912–3914; *Angew. Chem.* **2004**, *116*, 4002–4004.

[13] C. Y. Chow, H. Bolvin, V. E. Campbell, R. Guillot, J. W. Kampf, W. Wernsdorfer, F. Gendron, J. Autschbach, V. L. Pecoraro, T. Mallah, *Chem. Sci.* **2015**, *6*, 4148–4159.

[14] P. Happ, C. Plenk, E. Rentschler, *Coord. Chem. Rev.* **2015**, *289–290*, 238–260.

[15] Y. Pavlyukh, E. Rentschler, H. J. Elmers, W. Hübner, G. Lefkidis, *Phys. Rev. B* **2018**, *97*, 1–19.

[16] P. Happ, E. Rentschler, *Dalton Trans.* **2014**, *43*, 15308–15312.

[17] S. V. Eliseeva, E. V. Salerno, B. A. Lopez Bermudez, S. Petoud, V. L. Pecoraro, *J. Am. Chem. Soc.* **2020**, *142*, 16173–16176.

[18] E. R. Trivedi, S. V. Eliseeva, J. Jankolovits, M. M. Olmstead, V. L. Pecoraro, *J. Am. Chem. Soc.* **2014**, *136*, 1526–1534.

[19] C. Y. Chow, S. V. Eliseeva, E. R. Trivedi, T. N. Nguyen, J. W. Kampf, S. Petoud, V. L. Pecoraro, *J. Am. Chem. Soc.* **2016**, *138*, 5100–5109.

[20] T. N. Nguyen, S. V. Eliseeva, C. Y. Chow, J. W. Kampf, S. Petoud, V. L. Pecoraro, *Inorg. Chem. Front.* **2020**, *7*, 1553–1563.

[21] a) T. N. Nguyen, C. Y. Chow, S. V. Eliseeva, E. R. Trivedi, J. W. Kampf, I. Martinić, S. Petoud, V. L. Pecoraro, *Chem. Eur. J.* **2018**, *24*, 1031–1035; b) E. V. Salerno, J. Zeler, S. V. Eliseeva, M. A. Hernández-Rodríguez, A. N. Carneiro Neto, S. Petoud, V. L. Pecoraro, L. D. Carlos, *Chem. Eur. J.* **2020**, *26*, 13792–13796.

[22] J. C. Lutter, S. V. Eliseeva, G. Collet, I. Martinic, J. W. Kampf, B. L. Schneider, A. Carichner, J. Sobilo, S. Lerondel, S. Petoud, V. L. Pecoraro, *Chem. Eur. J.* **2019**, *26*, 1274–1277.

[23] J. Jankolovits, C. M. Andolina, J. W. Kampf, K. N. Raymond, V. L. Pecoraro, *Angew. Chem. Int. Ed.* **2011**, *50*, 9660–9664; *Angew. Chem.* **2011**, *123*, 9834–9838.

[24] J. Ferrando-Soria, J. Vallejo, M. Castellano, J. Martínez-Lillo, E. Pardo, J. Cano, I. Castro, F. Lloret, R. Ruiz-García, M. Julve, *Coord. Chem. Rev.* **2017**, *339*, 17–103.

[25] G. Aromí, F. Luis, O. Roubea, in *Lanthanides and Actinides in Molecular Magnetism*, (Eds.: R. A. Layfield, M. Murugesu), Wiley-VCH Verlap & Co. KGaA, Weinheim, Germany, **2015**; pp. 185–221.

[26] M. R. Azar, T. T. Boron III, J. C. Lutter, C. I. Daly, K. A. Zegalia, R. Nimthong, G. M. Ferrence, M. Zeller, J. W. Kampf, V. L. Pecoraro, C. M. Zaleski, *Inorg. Chem.* **2014**, *53*, 1729–1742.

[27] F. Cao, R.-M. Wei, J. Li, L. Yang, Y. Han, Y. Song, J. Dou, *Inorg. Chem.* **2016**, *55*, 5914–5923.

[28] J. R. Travis, A. M. Smihosky, A. C. Kauffman, S. E. Ramstrom, A. J. Lewis, S. G. Nagy, R. E. Rheam, M. Zeller, C. M. Zaleski, *J. Chem. Crystallogr.* **2021**, *51*, 372–393.

[29] C. M. Foley, M. A. Armanious, A. M. Smihosky, M. Zeller, C. M. Zaleski, *J. Chem. Crystallogr.* **2021**, *51*, 465–482.

[30] J. C. Lutter, B. A. Lopez Bermudez, T. N. Nguyen, J. W. Kampf, V. L. Pecoraro, *J. Inorg. Biochem.* **2019**, *192*, 119–125.

[31] J. Wang, J. Lu, Y. Liu, S.-G. Wu, G.-Z. Huang, J.-L. Liu, M.-L. Tong, *Cryst. Growth Des.* **2019**, *19*, 1896–1902.

[32] a) I. D. Brown, D. Altermatt, *Acta Crystallogr.* **1985**, *B41*, 244–247; b) N. E. Brese, M. O'Keeffe, *Acta Crystallogr.* **1991**, *B47*, 192–197; c) W. Liu, H. H. Thorp, *Inorg. Chem.* **1993**, *32*, 4102–4105; d) A. Trzesowska, R. Kruszynski, T. J. Bartezak, *Acta Crystallogr.* **2004**, *B60*, 174–178.

[33] a) M. Llunell, D. Casanova, J. Cirera, P. Alemany, S. Alvarez, *SHAPE*, ver. 2.1, Barcelona (Spain), **2013**; b) M. Pinsky, D. Avnir, *Inorg. Chem.* **1998**, *37*, 5575–5582; c) D. Casanova, J. Cirera, M. Llunell, P. Alemany, D. Avnir, S. Alvarez, *J. Am. Chem. Soc.* **2004**, *126*, 1755–1763; d) J. Cirera, E. Ruiz, S. Alvarez, *Organometallics* **2005**, *24*, 1556–1562.

[34] M. Perovic, V. Kusigerski, A. Spasojevic, V. Mrakovic, J. Blanusa, M. Zentkova, M. Mihalik, *J. Phys. D* **2013**, *46*, 165001.

[35] J. D. Rinehart, J. R. Long, *Chem. Sci.* **2011**, *2*, 2078–2085.

[36] C. Loosli, S.-X. Liu, A. Neels, G. Labat, S. Decurtins, *Z. Kristallogr. New Cryst. Struct.* **2006**, *221*, 135–141.

[37] a) N. Ishikawa, M. Sugita, T. Ishikawa, S. Koshihara, Y. Kaizu, *J. Am. Chem. Soc.* **2003**, *125*, 8694–8695; b) N. Ishikawa, M. Sugita, T. Ishikawa, S. Koshihara, Y. Kaizu, *J. Phys. Chem. B* **2004**, *108*, 11265–11271; c) N. Ishikawa, Y. Mizuno, S. Takamatsu, T. Ishikawa, S. Koshihara, *Inorg. Chem.* **2008**, *47*, 10217–10219.

[38] H. C. Brown, D. H. McDaniel, O. Häfliger in *Determination of Organic Structures by Physical Methods* (Eds.: E. A. Braude, F. C. Nachod), Academic Press Incs., **1955**; pp. 567–662.

[39] Bruker, Apex3 V2018.1-0, SAINT V8.38 A, Bruker AXS Inc., Madison (United States of America), **2018**.

[40] L. Krause, R. Herbst-Irmer, G. M. Sheldrick, D. Stalke, *J. Appl. Crystallogr.* **2015**, *48*, 3–10.

[41] G. M. Sheldrick, *Acta Crystallogr.* **2008**, *A64*, 112–122.

[42] G. M. Sheldrick, SHELXL2018, University of Göttingen, Göttingen (Germany), **2018**.

[43] G. M. Sheldrick, *Acta Crystallogr.* **2015**, *C71*, 3–8.

[44] C. B. Hübschle, G. M. Sheldrick, B. Dittrich, *J. Appl. Crystallogr.* **2011**, *44*, 1281–1284.

[45] P. Van Der Sluis, A. L. Spek, *Acta Crystallogr.* **1990**, *A46*, 194–201.

[46] A. L. Spek, *J. Appl. Crystallogr.* **2003**, *36*, 7–13.

[47] A. L. Spek, *Acta Crystallogr.* **2009**, *D65*, 148–155.

[48] L. J. Farrugia, *J. Appl. Crystallogr.* **2012**, *45*, 849–854.

[49] A. Lausi, M. Polentarutti, M. S. Onesti, J. R. Plaisier, E. Busetto, G. Bais, L. Barba, A. Cassetta, G. Campi, D. Lamba, A. Pifferi, S. C. Mande, D. D. Sarma, S. M. Sharma, G. Paolucci, *Eur. Physiscs J. Plus* **2015**, *130*, 43.

[50] W. Kabsch, *Acta Crystallogr.* **2010**, *D66*, 125–132.

[51] a) M. D. Winn, C. C. Ballard, K. D. Cowtan, E. J. Dodson, P. Emsley, P. R. Evans, R. M. Keegan, E. B. Krissinel, A. G. W. Leslie, A. McCoy, S. J. McNicholas, G. N. Murshudov, N. S. Pannu, E. A. Potterton, H. R. Powell, R. J. Read, A. Vagin, K. S. Wilson, *Acta Crystallogr.* **2011**, *D67*, 235–242; b) P. R. Evans, G. N. Murshudov, *Acta Crystallogr.* **2013**, *D69*, 1204–1214.

[52] O. V. Dolomanov, L. J. Bourhis, R. J. Gildea, J. A. K. Howard, H. Puschmann, *J. Appl. Crystallogr.* **2009**, *42*, 339–341.